

**This is a self-archived version of an original article. This version may differ from the original in pagination and typographic details.**

**Author(s):** Cao, LiAo; Mattelaer, Felix; Sajavaara, Timo; Dendooven, Jolien; Detavernier, Christophe

**Title:** A liquid alkoxide precursor for the atomic layer deposition of aluminum oxide films

**Year:** 2020

**Version:** Published version

**Copyright:** © 2020 Author(s)

**Rights:** In Copyright

**Rights url:** <http://rightsstatements.org/page/InC/1.0/?language=en>




**Please cite the original version:**

Cao, L., Mattelaer, F., Sajavaara, T., Dendooven, J., & Detavernier, C. (2020). A liquid alkoxide precursor for the atomic layer deposition of aluminum oxide films. *Journal of Vacuum Science and Technology A*, 38(2), Article 022417. <https://doi.org/10.1116/1.5139631>

# A liquid alkoxide precursor for the atomic layer deposition of aluminum oxide films

Cite as: J. Vac. Sci. Technol. A **38**, 022417 (2020); <https://doi.org/10.1116/1.5139631>

Submitted: 21 November 2019 . Accepted: 29 January 2020 . Published Online: 19 February 2020

LiAo Cao , Felix Mattelaer , Timo Sajavaara , Jolien Dendooven , and Christophe Detavernier 

## COLLECTIONS

Paper published as part of the special topic on [Special Topic Collection on Atomic Layer Deposition \(ALD\)](#)

Note: This paper is part of the 2020 Special Topic Collection on Atomic Layer Deposition (ALD).



View Online



Export Citation



CrossMark

## ARTICLES YOU MAY BE INTERESTED IN

[Surface reaction mechanisms during atomic layer deposition of zirconium oxide using water, ethanol, and water-ethanol mixture as the oxygen sources](#)

Journal of Vacuum Science & Technology A **38**, 012401 (2020); <https://doi.org/10.1116/1.5122994>

**HIDEN**  
ANALYTICAL

## Instruments for Advanced Science

Contact Hiden Analytical for further details:

**W** [www.HidenAnalytical.com](http://www.HidenAnalytical.com)

**E** [info@hiden.co.uk](mailto:info@hiden.co.uk)

**CLICK TO VIEW** our product catalogue



### Gas Analysis

- dynamic measurement of reaction gas streams
- catalysis and thermal analysis
- molecular beam studies
- dissolved species probes
- fermentation, environmental and ecological studies



### Surface Science

- UHV/TPD
- SIMS
- end point detection in ion beam etch
- elemental imaging - surface mapping



### Plasma Diagnostics

- plasma source characterization
- etch and deposition process reaction kinetic studies
- analysis of neutral and radical species



### Vacuum Analysis

- partial pressure measurement and control of process gases
- reactive sputter process control
- vacuum diagnostics
- vacuum coating process monitoring



# A liquid alkoxide precursor for the atomic layer deposition of aluminum oxide films

Cite as: J. Vac. Sci. Technol. A 38, 022417 (2020); doi: 10.1116/1.5139631

Submitted: 21 November 2019 · Accepted: 29 January 2020 ·

Published Online: 19 February 2020



LiAo Cao,<sup>1,a)</sup> Felix Mattelaer,<sup>1</sup> Timo Sajavaara,<sup>2</sup> Jolien Dendooven,<sup>1</sup> and Christophe Detavernier<sup>1</sup>

## AFFILIATIONS

<sup>1</sup>Department of Solid State Science, Ghent University, Krijgslaan 281 S1, 9000 Gent, Belgium

<sup>2</sup>Department of Physics, University of Jyväskylä, P.O. Box 35, FIN-40014 Jyväskylä, Finland

**Note:** This paper is part of the 2020 Special Topic Collection on Atomic Layer Deposition (ALD).

**a) Electronic mail:** [LiAo.Cao@UGent.be](mailto:LiAo.Cao@UGent.be)

## ABSTRACT

For large-scale atomic layer deposition (ALD) of alumina, the most commonly used alkyl precursor trimethylaluminum poses safety issues due to its pyrophoric nature. In this work, the authors have investigated a liquid alkoxide, aluminum tri-*sec*-butoxide (ATSB), as a precursor for ALD deposition of alumina. ATSB is thermally stable and the liquid nature facilitates handling in a bubbler and potentially enables liquid injection toward upscaling. Both thermal and plasma enhanced ALD processes are investigated in a vacuum type reactor by using water, oxygen plasma, and water plasma as coreactants. All processes achieved ALD deposition at a growth rate of 1–1.4 Å/cycle for substrate temperatures ranging from 100 to 200 °C. Film morphology, surface roughness, and composition have been studied with different characterization techniques.

Published under license by AVS. <https://doi.org/10.1116/1.5139631>

## I. INTRODUCTION

Aluminum oxide films are widely investigated due to their excellent chemical and thermal stability, high transparency, high breakdown voltage, and high resistivity. They are used as encapsulation layers,<sup>1–3</sup> barrier materials,<sup>4,5</sup> and dielectric films.<sup>6,7</sup> In such applications, coating a thin layer of aluminum oxide can suffice because of the excellent properties of these films. Among many commonly used methods for coating thin films, atomic layer deposition (ALD) can give excellent control of film thickness, stoichiometry, and conformality by a series of self-limited reactions.<sup>8</sup> Since the technique was first commercially used in depositing conformal ultrathin films for electroluminescent displays and microelectronics applications, more attention is drawn toward other applications, such as photovoltaics,<sup>9–11</sup> flexible electronics,<sup>12</sup> and powder coating.<sup>13</sup> Recent progress in reactor and process design ensures that large-area ALD is possible for those applications.<sup>14–16</sup> Compared to typical precursor consumption of ALD processes during microelectronics fabrication, the implementation of large-area ALD will increase precursor usage with a factor of 100 for roll-to-roll applications and up to four orders of magnitude for powder coatings, depending on the total volume of the powder bed.<sup>17</sup> Thus, safety for use and large-scale storage as well as a

reasonable cost are essential requirements for precursors used in large-area applications.

Trimethylaluminum (TMA) and its thermal process with water are the most commonly used precursor and process for ALD deposition of aluminum oxide, respectively.<sup>18–23</sup> TMA is a highly volatile and thermally stable chemical, and its high reactivity makes it an ideal precursor for ALD deposition with different coreactants over a wide range of temperatures. However, due to the direct metal–carbon bonding in the TMA molecule, TMA is also pyrophoric, toxic, corrosive, and moisture sensitive, which makes handling inconvenient. Many efforts have been taken to search for alternatives to TMA in ALD of aluminum oxide.  $\text{Me}_2\text{AlO}^i\text{Pr}$ ,<sup>24,25</sup>  $[\text{MeC}(\text{N}^i\text{Pr})_2]\text{AlEt}_2$ ,<sup>26</sup>  $\text{AlCl}_3$ ,<sup>27–30</sup>  $\text{AlEt}_3$ ,<sup>31</sup> and  $\text{Me}_2\text{AlCl}$  (Refs. 32 and 33) have been investigated during the past years. However, most of these alternative precursors can still raise safety, contamination, and cost problems in large-area applications.

Alkoxide precursors<sup>34,35</sup> can be a nonpyrophoric alternative to alkyls, as they only possess metal–oxygen bonds, not metal–carbon bonds. These chemicals have moderate thermal stability but are highly cost-effective when aiming for large-scale use. Alkoxide precursors, such as aluminum tri-isopropoxide (TIPA) and aluminum tri-ethoxide have been studied and used in chemical vapor

deposition (CVD).<sup>36,37</sup> Recently, we reported using TIPA as the aluminum source for ALD deposition of aluminum oxide.<sup>38</sup> Water, oxygen plasma, and water plasma were used as the oxygen source, and the processes generated high growth-per-cycle (GPC) and conformal thin films. However, TIPA is a solid precursor and it requires high source temperature to generate enough vapor into the reactor chamber for deposition. Though described as mildly toxic, aluminum tri-*sec*-butoxide (ATSB) is a stable liquid alkoxide precursor.<sup>39</sup> Its liquid nature suggests that it could be easier to generate enough vapor pressure at lower source temperature and could facilitate liquid injection for large-area applications<sup>40,41</sup> when very high precursor dosing is required. A recent paper researched ATSB for CVD and ALD deposition.<sup>42</sup> However, in that work, no ALD parameters such as saturation and temperature windows were reported and only the thermal process was reported.

In this work, we have performed an in-depth study on the plasma enhanced (PE)-ALD process characteristics and film properties using ATSB as a precursor. During thermal and plasma processes, we observe an apparent ALD growth window for  $\text{Al}_2\text{O}_3$  from 100 up to 300 °C. The growth rates achieved within the ALD window for all investigated processes are comparable to the typical rate that is achieved for thermal ALD using TMA and water (1.1 Å/cycle). However, it is also found that ATSB starts to decompose from 200 °C, although the decomposition rate appears quite limited for typical exposure doses until 300 °C. Scanning electron microscopy (SEM) and atomic force microscopy (AFM) images indicate a smooth surface of the deposited films from all processes. X-ray photoelectron spectroscopy (XPS) analysis confirms the stoichiometric deposition of  $\text{Al}_2\text{O}_3$  with carbon contamination below XPS detection limits (about 0.5 at. %) when an oxygen plasma was applied and only 1–2 at. % carbon for low-temperature  $\text{H}_2\text{O}$ -based thermal processes. The time-of-flight elastic recoil detection (ToF-ERD) confirms the presence of carbon impurities in the films deposited through thermal ALD and indicates varying degrees of hydrogen content in the deposited films depending on the process condition.

## II. EXPERIMENT

A home-built pump-type ALD reactor<sup>43</sup> is used for the process development of ATSB and several different reactants. ATSB was bought from Sigma-Aldrich with 97% purity. A glass bubbler with a stainless steel lid was used to contain the liquid ATSB, and water was stored in a stainless steel bottle. To generate sufficient vapor pressure, the water bottle was kept at room temperature, but the conveying line was heated to 80 °C in order to avoid condensation. The bubbler containing ATSB was heated until 100 °C to generate sufficient precursor vapor, and the transporting line was heated to 105 °C to avoid condensation. Argon gas was pulsed into the bubbler to carry precursor vapor into the reactor. Water, oxygen plasma, and water plasma were used as reactants in three deposition processes. A fused quartz column wrapped by a copper coil was placed on top of the chamber to generate plasma by connecting to a 13.56 MHz RF generator (ENI GHW-12Z). The remote plasma was set at 200 W and generated with an impedance matching network to minimize the reflected power.

The substrates used for deposition were Si (100) wafers with native oxide and cleaned by oxygen plasma to remove surface contamination before a process was started. During deposition, the Si substrate was placed on a copper block and heated evenly at a temperature varied from 100 to 300 °C. The pressure of the precursor pulse was controlled at  $5 \times 10^{-3}$  mbar with the turbo pump running. The pressure during the plasma pulse was also controlled at  $5 \times 10^{-3}$  mbar.

During deposition, a spectroscopic ellipsometer (J.A. Woollam M-200) was attached on the reactor to monitor aluminum oxide film growth *in situ*. The results were fitted with a Cauchy model for  $\text{Al}_2\text{O}_3$ , and the model parameters were optimized by inputting the final thickness of  $\text{Al}_2\text{O}_3$  oxide films measured *ex situ* with x-ray reflectivity (XRR). A Bruker D8 diffractometer using Cu K- $\alpha$  radiation was used to obtain XRR patterns. By fitting simulated patterns to measured ones, the analyses of the XRR patterns gave the information of the thickness and the films density. Films of about 20–30 nm thick deposited with water and plasma processes in 200 cycles were characterized by different methods. SEM was performed for surface imaging by an FEI Quanta 200F setup with a 10 keV electron beam energy. The surface morphology was determined by AFM with a Bruker Dimension Edge system operating in the tapping mode in air. XPS was conducted by using a Theta Probe system from Thermo Scientific using Al K $\alpha$  x rays generated at 15 kV and focusing to a spot size of 0.3 mm by an MXR1 monochromator gun to analyze the chemical composition of the films. Film samples were cleaned and etched by a short Ar plasma treatment to remove the surface carbon contamination and obtain the elemental depth profile during the XPS measurement. ToF-ERD was performed using a home-built spectrometer and a 1.7 MV Pelletron accelerator in Jyväskylä.<sup>44</sup> The incident particle beam for these measurements consisted of 11.915 MeV  $^{63}\text{Cu}^{6+}$  ions at an incoming angle of 10° and total scattering angle of 41°. The collected spectra were analyzed using in-house developed open source software called POTKU.<sup>45</sup>

## III. RESULTS AND DISCUSSION

To generate sufficient precursor vapor, the glass bubbler containing the ATSB was heated to 100 °C. Three coreactants were examined to react with the chemisorbed ATSB to generate deposition, i.e., water, oxygen plasma, and water plasma. *In situ* ellipsometry results confirmed linear growth as a function of the number of ALD cycles for all three processes when the sample temperature was 150 °C, as shown in Fig. 1(a). The dosing time of ATSB was 15 s and that of the coreactants was 5 s.

The processes were further investigated at various substrate temperatures, from 100 to 400 °C. To examine the presence of an unwanted CVD component, a process was run also without a coreactant. The GPC of the three processes and decomposition by only pulsing ATSB vapor are shown in Fig. 1(b), as a function of temperature. The dosing time was the same as that used in the linear growth tests. Based on the GPC values, the temperature range could be divided into three regions. At low temperature, no decomposition of ATSB is observed and the GPC of the three processes is stable around 1–1.4 Å/cycle. In

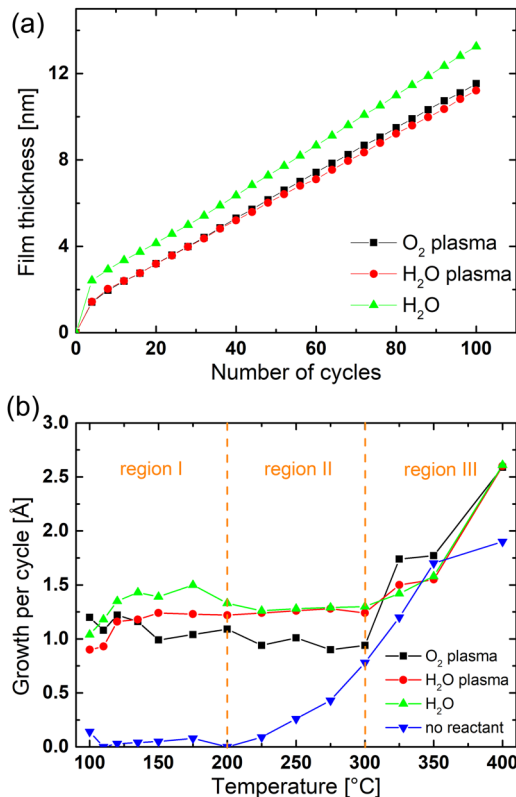


FIG. 1. (a) Linear growth behavior on the Si substrate at 150 °C, and (b) temperature windows of water, oxygen plasma, and water plasma process.

this region, the deposition is generated only by a self-limiting surface reaction of ATSB and coreactants. When the substrate is heated above 200 °C, the GPC behavior enters region II. The GPC of the ATSB and coreactants processes is still stable, but decomposition of ATSB is also initiated. This means, by a typical ATSB dosing time of 15 s, the decomposition is quite limited compared to the reaction with coreactants. Haanappel *et al.*<sup>46,47</sup> reported that from a temperature of 190 °C, the decomposition of ATSB is decomposing dominated by a  $\beta$ -hydride elimination mechanism and that a trace amount of water can contribute to the decomposition at high temperature. However, when we further increased the substrate temperature over 300 °C, the decomposition rate of ATSB takes off. The GPC in region III increased as the temperature increased and coincided with that of the decomposition. In this region, the deposition on the substrate is dominated by the decomposition of ATSB.

To ensure that the reaction in region I is a self-limited ALD deposition, the saturation behavior of both ATSB precursor and coreactants were investigated at the substrate temperature of 150 °C. First, the precursor test was done with 5 s coreactants pulse and the saturation [Fig. 2(a)] was achieved after a few seconds ATSB vapor pulse. Then, fixing the ATSB pulse time as 15 s, the growth was

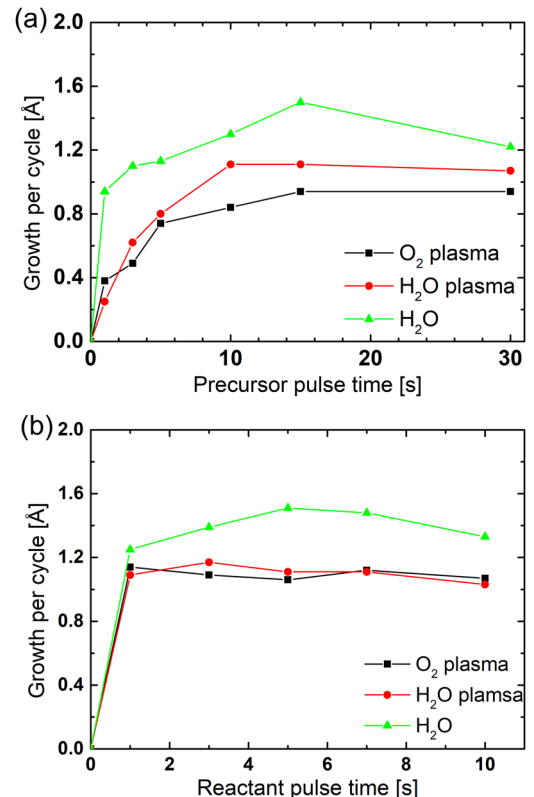
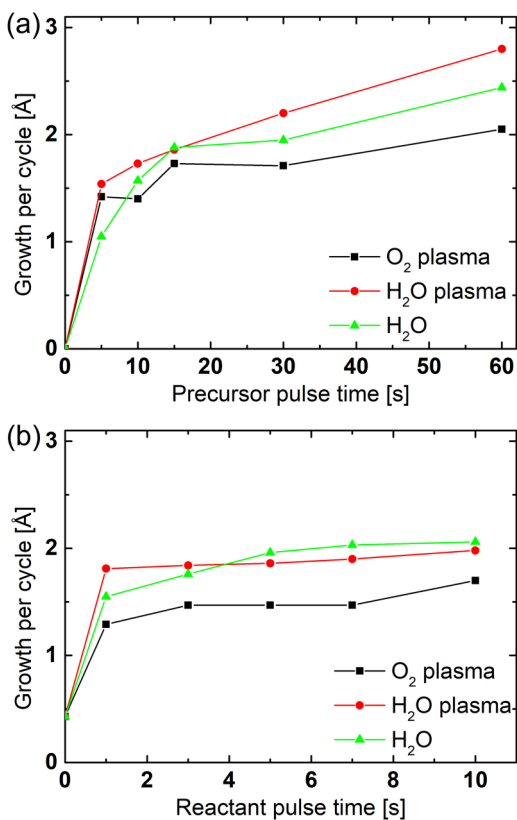


FIG. 2. Saturation curves at 150 °C: (a) 5 s coreactant pulse with different ATSB pulse time and (b) 15 s ATSB pulse with different pulse time for water, oxygen plasma, and water plasma.

also saturated [Fig. 2(b)] after 1 s coreactant pulse. The thermal process using water and the two plasma processes had a similar saturation behavior, and the results indicate that the deposition in region I is indeed ALD growth. The same saturation tests were also carried out at 275 °C (region II), as shown in Fig. 3. At this temperature, saturation could not be achieved [Fig. 3(a)] and the GPC kept increasing with longer precursor pulses, regardless of the coreactant species. When the precursor pulse time was fixed at 15 s, there was already some growth without involving any coreactants [Fig. 3(b)] due to the decomposition. The GPC increased when water or plasma was applied into the deposition and saturated, which is similar with the behavior of the coreactant pulse at 150 °C.

To investigate the quality of the films deposited by thermal and plasma ALD processes using ATSB, SEM and AFM studies were conducted on the films deposited at 150 °C substrate temperature. The results confirmed the deposition of smooth and uniform films when oxygen plasma [Figs. 4(a) and 4(d)], water plasma [Figs. 4(b) and 4(e)], and water [Figs. 4(c) and 4(e)] were used as coreactants with ATSB. The root mean square roughness was calculated from the AFM data and varied in value of 0.3–0.5 nm for all samples, indicating smooth layers.





**FIG. 3.** Saturation curve at 275 °C: (a) 5 s coreactant pulse with different ATSB pulse time and (b) 15 s ATSB pulse with different pulse time for water, oxygen plasma, and water plasma.

To investigate the composition of the aluminum oxide films deposited in regions I and II, XPS was carried out on samples deposited with three coreactants at substrate temperatures of 100, 150, and 275 °C. As shown in Figs. 5(a) and 5(b), Al and O signals indicate the deposition of an alumina film. The carbon peak from the as-deposited film disappeared after Ar plasma etching in the surface, suggesting that only a small content of carbon is present in the films. However, when we look closely into the carbon peak position after etching, a very weak carbon peak was still present [Fig. 5(c)] for samples grown with the water thermal process at 100 and 150 °C. The spectra near the carbon position after etching are shown in Fig. 6 for samples in five deposition conditions, i.e., the thermal process at 100, 150, and 275 °C and the PE-ALD process at 150 °C. The figure shows that carbon is indeed present in the thermally grown films using water at low temperature, i.e., at 100 and 150 °C. The XPS measured concentration of carbon in the water thermal process sample at 100 and 150 °C was approximately 0.5 at.%, which is near the detection limit of XPS. The position of the carbon peak is around 289.3 eV (Ref. 48) and can be signed to C–O bonds. The result indicates that at low temperature, a water molecule is not active enough to

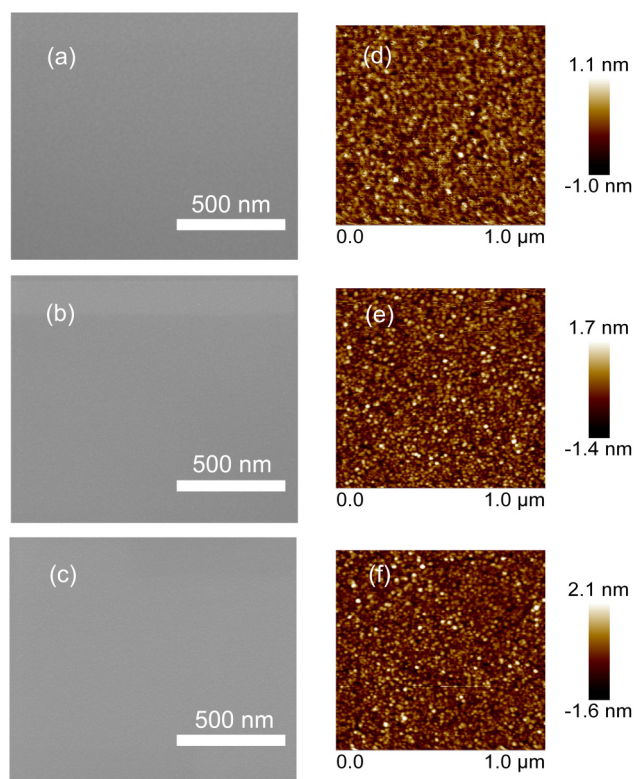


**FIG. 4.** SEM and AFM images of aluminum oxide films deposited at 150 °C using oxygen plasma [(a) and (d)], water plasma [(b) and (e)], and water [(c) and (f)] as coreactants.

replace all the alkoxy ligands of the precursor. In the ALD regime in region I by using plasma as the coreactant, no carbon was detected by XPS, indicating superior purity even at 100 °C within the ALD regime. Finally, when a higher temperature was used for the thermal process, i.e., 275 °C, in region II in Fig. 1(b), no carbon was detected. However, the reader must note that this process is no longer truly ALD, and the CVD component will challenge the conformality aspect of the films and limit the upscalability.

Since XPS cannot detect hydrogen, commonly found as an impurity in ALD films originating from the remaining ligands or absorbed water, ToF-ERD was used to determine the hydrogen content and provide a more sensitive detection for light elements such as carbon and oxygen. Six samples were selected: water thermal ALD films at 150, 200, and 275 °C and oxygen plasma ALD films at the same temperatures. As shown in Table I, ToF-ERD analysis confirms the low carbon content revealed by the XPS results. Thermal ALD film results in 0.7–1.3 at. % carbon content, depending on the deposition temperature. For plasma-based films, the carbon content is below the detection limit of ToF-ERD (<0.2 at. %) for this type of below 30 nm thick films. A small amount of Ti was detected in the films. The Ti signal is most likely originating from contamination of the precursor

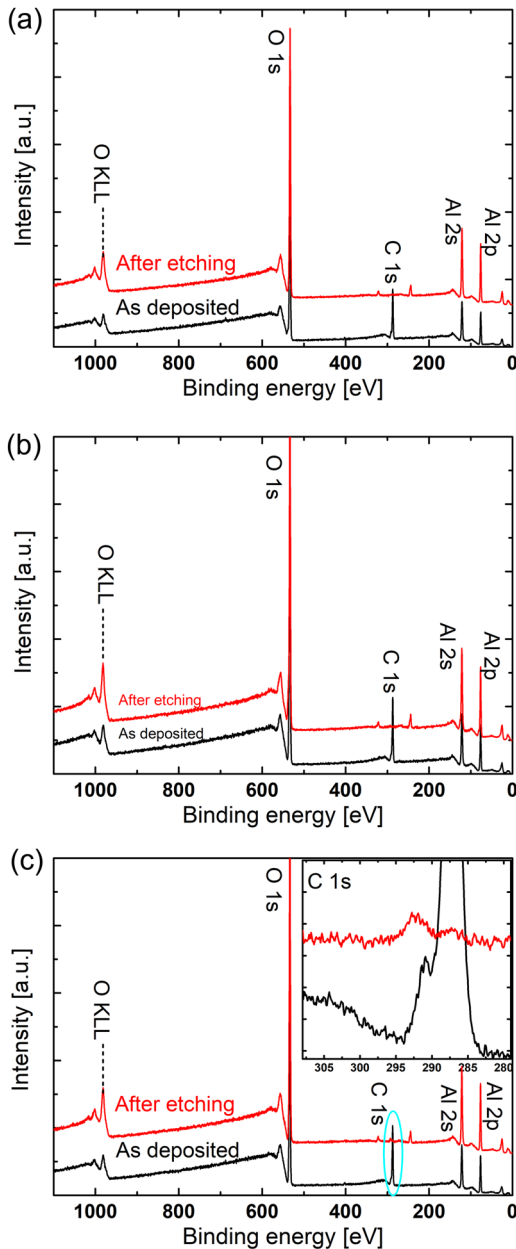


FIG. 5. XPS spectra of aluminum oxide films deposited at 150 °C with (a) oxygen plasma, (b) water plasma, and (c) water as coreactants.

conveying tube, since there is no Ti source in the ALD reaction system.

Furthermore, the hydrogen content in films from the plasma process is relatively stable from 8.2 to 6.1 at. % as the temperature increases. The oxygen plasma tends to combust all ligands, which leaves a very low carbon trace and some hydrogen residue. The combustion effect does not change as the temperature increases.

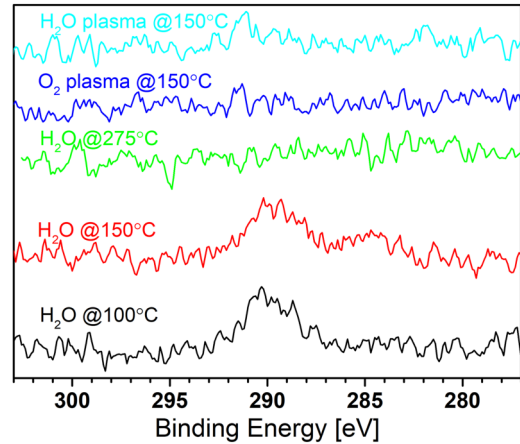


FIG. 6. The carbon details from XPS spectra of films deposited at different temperatures with different coreactants.

The hydrogen content cannot originate from  $-CH_3$  residue in the films, due to the low carbon content. This suggests that hydrogen is present in the film in the form of  $-OH$  groups or water molecules. While the stoichiometry of the films from the plasma process is close to what is expected for aluminum oxide with 60 at. % oxygen, Al is slightly lower than 40 at. %. After subtracting the O amount for the  $-OH$  groups, based on the measured H, and Ti impurities, the Al:O ratio is indeed close to that of stoichiometric aluminum oxide. Surprisingly, there is even less hydrogen content in the thermal process with water at 275 °C. The reaction in region II may already go toward decomposition at 275 °C, supporting that hydrogen must be removed during the decomposition. However, for thermal based samples in region I, a much higher hydrogen content (17–19 at. %) was observed. The carbon impurities in these films suggest the presence of  $-CH_x$  groups, and the C is from the remaining alkoxy ligands according to the XPS analysis. But since the measured H:C ratio is larger than 3:1,  $-OH$  groups are also present in these films. By assuming that C and H are present in these forms in the films, the corrected Al:O ratio is again in agreement with stoichiometric aluminum oxide.

TABLE I. Atomic concentrations in the central region of the deposited films (conditions as below), not considering interface effects at the surface or silicon interface, as calculated from the ToF-ERD measurements using POTKU software.

	O (at. %)	Al (at. %)	H (at. %)	C (at. %)	Ti (at. %)
H <sub>2</sub> O ALD, 150 °C	53 ± 4	25 ± 3	19 ± 2	1.3 ± 0.3	0.9 ± 0.2
H <sub>2</sub> O ALD, 200 °C	54 ± 3	29 ± 2	17 ± 2	0.7 ± 0.2	0.4 ± 0.1
H <sub>2</sub> O ALD, 275 °C	60 ± 4	36 ± 3	1.9 ± 0.5	0.8 ± 0.3	0.7 ± 0.2
O <sub>2</sub> PE-ALD, 150 °C	58 ± 3	32 ± 2	8.2 ± 0.8	<0.2	1.7 ± 0.2
O <sub>2</sub> PE-ALD, 200 °C	55 ± 3	34 ± 3	7.5–12.5	<0.2	0.9 ± 0.1
O <sub>2</sub> PE-ALD, 275 °C	59 ± 3	34 ± 3	6.1 ± 1.0	<0.2	0.8 ± 0.1

#### IV. SUMMARY AND CONCLUSIONS

ATSB was demonstrated as a liquid, nonpyrophoric alkoxide-type precursor for ALD of aluminum oxide. Thermal ALD with water and plasma enhanced ALD with water plasma and oxygen plasma produced smooth, uniform, and near-stoichiometric Al<sub>2</sub>O<sub>3</sub> layers. The GPC of the three processes was 1.0–1.4 Å/cycle from 100 to 300 °C. A detailed investigation of the saturation behavior and thermal decomposition of ATSB indicated real ALD conditions for a substrate temperature of 100 to 200 °C, while some parasitic CVD-type decomposition occurred from 200 to 300 °C. For thermal ALD with H<sub>2</sub>O as a coreactant, the films contained 0.7–1.3 at. % carbon contamination and 17–19 at. % hydrogen for deposition at 100–200 °C or 1.9 at. % hydrogen at 275 °C. For plasma enhanced ALD with O<sub>2</sub> plasma as a coreactant, carbon contamination was below the detection limit of both XPS and ToF-ERD, while ERD indicated approximately 6.1–8.2 at. % hydrogen impurities.

#### ACKNOWLEDGMENTS

This work was supported by the M-ERA CALDERA project and the Fund for Scientific Research Flanders (FWO). Jolien Dendooven acknowledges the FWO for a postdoctoral fellowship.

#### REFERENCES

- <sup>1</sup>Y. Q. Yang, Y. Duan, P. Chen, F. B. Sun, Y. H. Duan, X. Wang, and D. Yang, *J. Phys. Chem. C* **117**, 20308 (2013).
- <sup>2</sup>H. Y. Li, Y. F. Liu, Y. Duan, Y. Q. Yang, and Y. N. Lu, *Materials* **8**, 600 (2015).
- <sup>3</sup>Y. Liu, J. Tolentino, M. Gibbs, R. Ihly, C. L. Perkins, Y. Liu, N. Crawford, J. C. Hemminger, and M. Law, *Nano Lett.* **13**, 1578 (2013).
- <sup>4</sup>P. Poedt, A. Lankhorst, F. Roozeboom, K. Spee, D. Maas, and A. Vermeer, *Adv. Mater.* **22**, 3564 (2010).
- <sup>5</sup>L. J. Antila *et al.*, *J. Phys. Chem. C* **115**, 16720 (2011).
- <sup>6</sup>J. H. Chang, D. Y. Choi, S. Han, and J. J. Pak, *Microfluid. Nanofluid.* **8**, 269 (2010).
- <sup>7</sup>M. Wang, X. Li, X. Xiong, J. Song, C. Gu, D. Zhan, Q. Hu, S. Li, and Y. Wu, *IEEE Electron Device Lett.* **40**, 419 (2019).
- <sup>8</sup>V. Cremers, R. L. Puurunen, and J. Dendooven, *Appl. Phys. Rev.* **6**, 021302 (2019).
- <sup>9</sup>T. R. B. Foong, Y. Shen, X. Hu, and A. Sellinger, *Adv. Funct. Mater.* **20**, 1390 (2010).
- <sup>10</sup>I. S. Kim, R. T. Haasch, D. H. Cao, O. K. Farha, J. T. Hupp, M. G. Kanatzidis, and A. B. F. Martinson, *ACS Appl. Mater. Interfaces* **8**, 24310 (2016).
- <sup>11</sup>J. A. Van Delft, D. Garcia-Alonso, and W. M. M. Kessels, *Semicond. Sci. Technol.* **27**, 074002 (2012).
- <sup>12</sup>P. Poedt, R. Knaapen, A. Illiberi, F. Roozeboom, and A. van Asten, *J. Vac. Sci. Technol. A* **30**, 01A142 (2012).
- <sup>13</sup>B. J. O'Neill *et al.*, *ACS Catal.* **5**, 1804 (2015).
- <sup>14</sup>D. Longrie, D. Deduytsche, and C. Detavernier, *J. Vac. Sci. Technol. A* **32**, 010802 (2014).
- <sup>15</sup>H. Van Bui, F. Grillo, and J. R. Van Ommen, *Chem. Commun.* **53**, 45 (2017).
- <sup>16</sup>H. Tiznado, D. Domínguez, F. Muñoz-Muñoz, J. Romo-Herrera, R. Machorro, O. E. Contreras, and G. Soto, *Powder Technol.* **267**, 201 (2014).

- <sup>17</sup>E. Granneman, P. Fischer, D. Pierreux, H. Terhorst, and P. Zagwijn, *Surf. Coat. Technol.* **201**, 8899 (2007).
- <sup>18</sup>V. Miikkulainen, M. Leskelä, M. Ritala, and R. L. Puurunen, *J. Appl. Phys.* **113**, 021301 (2013).
- <sup>19</sup>S. M. George, *Chem. Rev.* **110**, 111 (2010).
- <sup>20</sup>R. L. Puurunen, *J. Appl. Phys.* **97**, 121301 (2005).
- <sup>21</sup>M. Leskelä and M. Ritala, *Angew. Chem Int. Ed.* **42**, 5548 (2003).
- <sup>22</sup>M. Leskelä and M. Ritala, *Thin Solid Films* **409**, 138 (2002).
- <sup>23</sup>S. M. George, A. W. Ott, and J. W. Klaus, *J. Phys. Chem.* **100**, 13121 (1996).
- <sup>24</sup>W. Cho, K. Sung, K.-S. An, S. Sook Lee, T.-M. Chung, and Y. Kim, *J. Vac. Sci. Technol. A* **21**, 1366 (2003).
- <sup>25</sup>S. E. Potts, G. Dingemans, C. Lachaud, and W. M. M. Kessels, *J. Vac. Sci. Technol. A* **30**, 021505 (2012).
- <sup>26</sup>A. L. Brazeau and S. T. Barry, *Chem. Mater.* **20**, 7287 (2008).
- <sup>27</sup>S. Dueñas *et al.*, *J. Appl. Phys.* **99**, 054902 (2006).
- <sup>28</sup>M. Ritala, H. Saloniemi, M. Leskelä, T. Prohaska, G. Friedbacher, and M. Grasserbauer, *Thin Solid Films* **286**, 54 (1996).
- <sup>29</sup>S. J. Yun, K.-H. Lee, J. Skarp, H.-R. Kim, and K.-S. Nam, *J. Vac. Sci. Technol. A* **15**, 2993 (1997).
- <sup>30</sup>M. Tiitta, E. Nykänen, P. Soininen, L. Niinistö, M. Leskelä, and R. Lappalainen, *Mater. Res. Bull.* **33**, 1315 (1998).
- <sup>31</sup>R. Huang and A. H. Kitai, *Thin Solid Films* **22**, 215 (1993).
- <sup>32</sup>S. Li, Y. Bao, M. Laitinen, T. Sajavaara, M. Putkonen, and H. Savin, *Phys. Status Solidi A* **212**, 1795 (2015).
- <sup>33</sup>K. Kukli, M. Ritala, M. Leskelä, and J. Jokinen, *J. Vac. Sci. Technol. A* **15**, 2214 (1997).
- <sup>34</sup>D. C. Bradley and M. M. Faktor, *J. Appl. Chem.* **9**, 435 (1959).
- <sup>35</sup>D. C. Bradley and J. M. Thomas, *Philos. Trans. R. Soc. A Math. Phys. Eng. Sci.* **330**, 167 (1990).
- <sup>36</sup>S. Blittersdorf, N. Bahlawane, K. Kohse-Höinghaus, B. Atakan, and J. Müller, *Chem. Vap. Depos.* **9**, 194 (2003).
- <sup>37</sup>L. Hiltunen, H. Kattelus, M. Leskelä, M. Mäkelä, L. Niinistö, E. Nykänen, P. Soininen, and M. Tiittad, *Mater. Chem. Phys.* **28**, 379 (1991).
- <sup>38</sup>F. S. M. Hashemi, L. Cao, F. Mattelaer, T. Sajavaara, J. R. van Ommen, and C. Detavernier, *J. Vac. Sci. Technol. A* **37**, 040901 (2019).
- <sup>39</sup>G. P. Shulman, M. Trusty, and J. H. Vickers, *J. Org. Chem.* **28**, 907 (1963).
- <sup>40</sup>R. J. Potter, P. R. Chalker, T. D. Manning, H. C. Aspinall, Y. F. Loo, A. C. Jones, L. M. Smith, G. W. Critchlow, and M. Schumacher, *Chem. Vap. Depos.* **11**, 159 (2005).
- <sup>41</sup>P. R. Chalker, S. Romani, P. A. Marshall, M. J. Rosseinsky, S. Rushworth, and P. A. Williams, *Nanotechnology* **21**, 405602 (2010).
- <sup>42</sup>X. Xia, A. Taylor, Y. Zhao, S. Guldin, and C. Blackman, *Materials* **12**, 1429 (2019).
- <sup>43</sup>T. Dobbelaere, F. Mattelaer, A. K. Roy, P. Vereecken, and C. Detavernier, *J. Mater. Chem. A* **5**, 330 (2017).
- <sup>44</sup>M. Laitinen, M. Rossi, J. Julin, and T. Sajavaara, *Nucl. Instrum. Methods Phys. Res. Sect. B* **337**, 55 (2014).
- <sup>45</sup>K. Arstila *et al.*, *Nucl. Instrum. Methods Phys. Res. Sect. B* **331**, 34 (2014).
- <sup>46</sup>V. A. C. Haanappel, H. D. van Corbach, T. Fransen, and P. J. Gellings, *Thermochim. Acta* **240**, 67 (1994).
- <sup>47</sup>V. A. C. Haanappel, H. D. van Corbach, T. Fransen, and P. J. Gellings, *Thin Solid Films* **230**, 138 (1993).
- <sup>48</sup>J. L. Hueso, J. P. Espinós, A. Caballero, J. Cotrino, and A. R. González-Elipe, *Carbon* **45**, 89 (2007).